International Journal of Chemical Science
www.chemicaljournals.com
E-ISSN: 2523-2843
Received: 28-09-2026, Accepted: 28-10-2026, Published: 12-11-2026
Volume 10, Issue 4, 2026, Page No. 4-13

Photocatalytic degradation of ternary composite through dual Z-scheme

Mansi Garbada*, Seema Kothari
Department of Chemistry, PAHER University, Udaipur, Rajasthan, India
Corresponding Author: Mansi Garbada
DOI: https://doi.org/10.66856/chemical.2026.10.4.10061

Abstract
The current study investigates the preparation of a ternary composite g-C_3N_4/WO_3/Bi_2O_3 for removal of Evans Blue dye (EB) dye via dual Z scheme. The composite was fabricated by hydrothermal-calcination method. It is a nanocomposite as its particle size was observed 100nm. The dye Evans Blue was degraded by as prepared composite under following optimized conditions such as pH 8.0, concentration of dye 0.4 mg/L, amount of catalyst 0.06 g/100 mL, and light intensity 60 mWcm^{-2}. The ternary photocatalyst achieved 89.75% degrade EB within 190 min. The synthesized nanocomposite was confirmed by X-ray diffraction (XRD), UV- Vis spectroscopy, Fourier-Transform Infrared Spectroscopy (FTIR) and Scanning Electron Microscopy (SEM) studies.

Highlights:
- A hydrothermal-calcination method was used to fabricate g-C_3N_4/WO_3/Bi_2O_3.
- Enhanced charge separation rate because of dual Z-scheme pathway.
- •O^{2-} and •OH are active reactive species in photo degradation.

Keywords: Dual Z-scheme, g-C_3N_4/WO_3/Bi_2O_3, Evans Blue (EB), hydrothermal, calcination, nanocomposite, photocatalyst

Introduction
Environment pollution is a very serious problem affecting environment and health in different ways. The discharge of untreated dye effluents from printing, textile, dyeing, tanning, pharmaceutical industries, etc. constitutes one of the most visible and chemically persistent forms of water pollution. Fujishima and Honda (1972) [2], studied about the basic principle of photogenerated electron–hole pairs. Earlier studies by Ameta *et al.* (2011) [11] on Naphthol Green B dye degradation using semiconducting antimony trisulfide emphasized the critical role of semiconductor in efficient photocatalytic systems. Zhang *et al.* (2014) [6] prepared binary composite g-C_3N_4–Bi_2O_3 via direct Z scheme photocatalyst. Diazo dyes produce highly toxic aromatic amine, which can cause human diseases as they show properties such as resistance acid, alkali, microbe (Navarro, *et al*., 2017). Jiang *et al*. (2018) [7] investigated synthesis of ternary combination of g-C_3N_4, WO_3, and Bi_2O_3 for the decomposition of non-biodegradable refractory pollutants by direct solid-state dual Z-scheme.
The environmental pollution caused various dyes is increasingly becoming serious (Martínez-López, *et al*., 2019; Yang *et al*., 2023) [5, 13]. The decomposition of dyes may be completed by ternary composited via dual Z scheme. The dual Z scheme permits photogenerated electrons of one semiconductor to selectively recombine with holes of the other at the interface. Dual and multiple Z-scheme ternary structures improves charge separation, superior visible– light activity (Li *et al*., 2024; Zheng *et al*., 2026). Boddepalli *et al.* (2026) [12, 17] observed experiment results for the effective environmental remediation of next-generation dual Z-scheme hetero structured photocatalysts.
Sher *et al*., (2021) [9] fabricated g-C_3N_4/Cd-doped ZnO nanocomposites for degradation and disinfection of organic pollutants in the presence of visible light irradiation. Basirun *et al*. (2023) [1] developed a method for removal of EB dye by using a cheap durian husk biosorbent. This dye was degraded (95.95%) with 72.0 mg/g adsorption amount at pH 2. Mostafa *et al*. (2024) [8] synthesized forsterite nanoparticles than used as an adsorbent for this dye. As-prepared 0.1 g of composite absorb 10 ppm of dye (EB dye) with in ten minutes at a pH 3.
Abdollahpour and Bazyari (2025) [10] fabricated a high-surface-area g-C_3N_4/TiO_2–WO_3–Bi_2O_3/SiO_2 nanocomposites which depicts improved visible-light-driven degradation of organic dyes. Wang *et al*. (2025) [20] used WO_3/BiOBr/g-C_3N_4 composite for the photocatalytic degradation of tetracycline antibiotic. Galavidoost *et al*., (2026) [18] synthesized rich TiO_{2-} x with WS_2/Co_3S_4/Co_9S_8 for the photocatalytic degradation of effluents via dual Z-scheme and also studied about the global issue of growing shortage of clean drinking water.
The present study covers (i) synthesis of a ternary composite g-C_3N_4/WO_3/Bi_2O_3 (ii) characterization of synthesized composite (iii) degradation of dye by various parameters (iv) results and discussion.

Materials and Methods
1. Chemicals and Reagents
All chemicals were of analytical reagent grade and used as received without any further purification. Melamine (≥99%), sodium tungstate dihydrate ($Na_2WO_4.2H_2O$), bismuth(III) nitrate pentahydrate ($Bi(NO_3)_3 \cdot 5H_2O$, ≥98%), and Evans blue dye were purchased from HiMedia Laboratories Pvt. Ltd. (Mumbai, India). Sodium hydroxide (NaOH) and sulfuric acid (H_2SO_4) were used for pH adjustment. Deionized water was used throughout all the experiments.

2. Synthesis of Photocatalysts

2.1 Synthesis of g-C_3N_4

Graphitic carbon nitride (g-C_3N_4) was synthesized by the thermal polycondensation of melamine. Briefly, 10 g of melamine was placed in a covered alumina crucible and heated in a muffle furnace gradually increasing temperature from room temperature till 550 °C at a constant heating rate of 5 °C min^{-1}. The temperature was maintained at 550 ± 5 °C for 4 h. After naturally cooling to room temperature, the resulting yellow product was ground into a fine powder and designated as pure g-C_3N_4.

2.2 Synthesis of WO_3

WO_3 was synthesized using precipitation method followed by thermal annealing. A 20 mL aqueous solution of $Na_2WO_4 \cdot 2H_2O$ (0.227 M) was acidified by the dropwise addition of 15 mL of 4 M HCl under continuous stirring until a yellow precipitate formed. The suspension was stirred for 4 h and then aged for 20 h at room temperature. The precipitate was collected by filtration, washed thoroughly with deionized water followed by ethanol until it gets free from chloride ions, and dried at 60 °C for 12 h. The dried powder was subsequently annealed at 450 °C for 2 h (heating rate: 5 °C min^{-1}) to obtain crystalline WO_3. After cooling to room temperature, the product was ground into a fine powder and stored in a desiccator until further use.

2.3 Synthesis of Bi_2O_3

Bi_2O_3 was synthesized by the thermal decomposition of bismuth(III) nitrate pentahydrate. Briefly, 9.7 g of $Bi(NO_3)_3 \cdot 5H_2O$ was dissolved in 100 mL of dilute nitric acid (HNO_3 = 1:9, v/v), followed by the addition of 1 g of polyethylene glycol (PEG-100) as a dispersing agent. A 0.5 M NaOH solution was then added dropwise under continuous stirring until complete precipitation occurred. The resulting suspension was stirred for an additional 2 h, and the precipitate was separated by centrifugation, washed several times with deionized water and ethanol, and dried at 80 °C. The dried material was calcined in a muffle furnace at 400 °C for 2 h maintaining a heating rate of 5 °C min^{-1} to obtain fine yellow crystalline Bi_2O_3 powder.

2.4 Synthesis of g-C_3N_4/WO_3/Bi_2O_3 Ternary Composite

The g-C_3N_4/WO_3/Bi_2O_3 ternary composite was synthesized by calcination method adapted from Jiang *et al.* (2018) [7]. 5.0 g melamine, 0.3 g tungstic acid (H_2WO_4) and 0.3 g bismuth(III) nitrate pentahydrate [$Bi(NO_3)_3 \cdot 5H_2O$] were mixed. They were thoroughly ground in an agate mortar for 30 min to obtain a homogeneous mixture. The resulting mixture was transferred to a covered alumina crucible and calcined in air at 520 °C for 2 h, then increased to 540°C for another 2 h at a heating rate of 5 °C min^{-1}. After naturally cooling at room temperature, the obtained yellowish powder was finely grounded and stored in a desiccator for subsequent characterization and photocatalytic degradation experiments.

3. Characterization

The crystal structure and phase purity of the synthesized g-C_3N_4/WO_3/Bi_2O_3 composite were examined by X-ray diffraction (XRD) using a Malvern Empyrean diffractometer. The functional groups and chemical bonding were analyzed by Fourier transform infrared spectroscopy (FTIR) using a Thermo Scientific Nicolet Summit X spectrometer in the wavenumber range of 400–4000 cm^{-1}. The surface morphology and microstructure of the photocatalyst were investigated using a Hitachi SU8010 Series field-emission scanning electron microscope (FESEM), while the elemental composition was determined by Energy-Dispersive X-ray Spectroscopy (EDS) using a Thermo Scientific Flash 2000 analyzer. The optical absorption properties of the synthesized photocatalyst were evaluated by UV–visible diffuse reflectance spectroscopy (UV–vis DRS) using a JASCO V-750 spectrophotometer (Japan). The characterization techniques employed and their respective purposes are summarized in Table 1.

Table 1: Characterization techniques used for the synthesized g-C_3N_4/WO_3/Bi_2O_3 composite.

S. No.	Type of Analysis	Characterization
1	X-ray diffraction (XRD)	Phase identification and crystal structure analysis
2	Fourier transform infrared spectroscopy (FTIR)	Functional group and chemical bond analysis
3	Field emission scanning electron microscopy (FESEM)	Surface morphology
4	Energy dispersive spectroscopy (EDS)	Elemental composition
5	UV-Vis diffuse reflectance spectra (DRS)	Optical properties and band-gap estimation

4. Photocatalytic Degradation Experiments

Photocatalytic degradation experiments were carried out in a 250 mL cylindrical Pyrex photoreactor equipped with a water-cooling jacket to maintain the reaction temperature at 25 ± 1 °C. A tungsten filament lamp (20–70 W) was used as the visible-light source and positioned 10 cm above the reaction vessel. In a typical experiment, the required amount of photocatalyst was dispersed in 100 mL of Evans Blue solution of known concentration. Prior to light irradiation, the suspension was magnetically stirred in the dark for 30 min to establish adsorption–desorption equilibrium between the dye molecules and the catalyst surface.

During irradiation, 3 mL aliquots were withdrawn at regular time intervals and centrifuged at 5000 rpm for 5 min to remove suspended catalyst particles. The absorbance of the clear supernatant was measured at the maximum absorption wavelength (λ_max = 608- 620 nm) using a UV–Vis spectrophotometer.

The degradation efficiency (%) and pseudo-first-order rate constant (k) were calculated using:

$$\text{Degradation rate (\%)} = \left[\frac{A_0 - A_t}{A_0}\right] \times 100$$

Where $\mathbf{A_0}$ and $\mathbf{A_t}$ represent the absorbance at irradiation times 0 and *t*, respectively.

The apparent pseudo-first-order rate constant (**k**) was determined using the Langmuir–Hinshelwood kinetic model:

$$\ln(A_0/A_t) = kt \text{ or } (1 + \log A) = (1 + \log A_0) - kt/2.303$$

Where A_0 and A_t are the absorbances at time 0 and time t, respectively, and k is the apparent pseudo-first-order rate constant (s^{-1}).

Parametric Optimization

The photocatalytic performance of the g-C_3N_4/WO_3/Bi_2O_3 composite was evaluated by varying one experimental parameter while keeping the remaining parameters constant are as mentioned.

- Solution of pH: 5.0–10.0 (adjusted using 0.1 M NaOH or HCl)
- Initial Evans blue concentration: 0.2–1.4 mg L^{-1}
- Catalyst dosage: 0.02–0.12 g per 100 mL
- Light intensity: 20–70 mW cm^{-2}

The optimum operating conditions were determined from the apparent pseudo-first-order rate constants obtained under each experimental condition.

Results and Discussion

1. Characterization of g-C_3N_4 /WO_3/Bi_2O_3

1.1 X-ray Diffraction Analysis (XRD)

The crystalline phases and structural properties of the synthesized g-C_3N_4/WO_3/Bi_2O_3 ternary composite were investigated by X-ray diffraction (XRD), and the corresponding diffraction pattern is presented in Figure 1. The characteristic diffraction peaks observed in the composite confirm the successful formation of the heterojunction while preserving the individual crystal structures of the constituent semiconductors. The diffraction peaks located at 13.1° and 27.4° correspond to the (100) and (002) crystallographic planes of graphitic carbon nitride (g-C_3N_4), respectively. The weak reflection at 13.1° is attributed to the in-plane structural packing of tri-s-triazine units, whereas the intense peak at 27.4° originates from the interlayer stacking of conjugated aromatic layers, confirming the successful formation of graphitic carbon nitride (Wang *et al.* 2009; Ong *et al.* 2016) [14, 16].

The diffraction peaks observed at 23.1°, 23.6°, 24.4°, 33.6°, 34.2°, 41.7°, 49.9°, 55.9°, and 62.2° are assigned to the characteristic crystal planes of monoclinic WO_3, which are in good agreement with the reported standard diffraction data (Fernandes *et al.* 2022) [4]. Similarly, the diffraction peaks appearing at 27.5°, 33.0°, 46.3°, 54.2°, and 57.6° correspond to the characteristic planes of monoclinic α-Bi_2O_3, confirming its crystalline nature (Berekute *et al.* 2022) [3].

The XRD pattern of the ternary composite exhibits diffraction peaks corresponding to all three constituent materials without the appearance of additional impurity peaks, indicating that the co-calcination process did not generate any undesirable secondary phases. Although the characteristic peak of g-C_3N_4 at 27.4° partially overlaps with the diffraction peaks of WO_3 and Bi_2O_3, its presence together with the characteristic reflections of the metal oxides confirms the successful incorporation of all components into the composite. The slight reduction in the intensity of the g-C_3N_4 reflections compared with pristine g-C_3N_4 can be attributed to the intimate interaction between g-C_3N_4 sheets and the WO_3/Bi_2O_3 particles, which promotes the formation of a well-contacted heterojunction while preserving the crystal structures of the individual phases.

The absence of any noticeable peak shifts or additional diffraction peaks further indicates that no new crystalline phase was formed during calcination. Instead, the enhanced photocatalytic performance of the composite is mainly attributed to the interfacial coupling between g-C_3N_4, WO_3, and Bi_2O_3, which facilitates efficient charge transfer across the heterojunction rather than changes in crystal structure. Similar observations have been reported for g-C_3N_4-based ternary heterojunction photocatalysts synthesized via co-calcination methods (Jiang *et al.* 2018; Wang *et al.* 2024; Wang *et al.* 2025) [7, 15, 20].

Overall, the XRD results demonstrate that the synthesized g-C_3N_4/WO_3/Bi_2O_3 composite possesses high crystallinity and phase purity, confirming the successful fabrication of the ternary heterojunction required for enhanced visible-light photocatalytic activity.

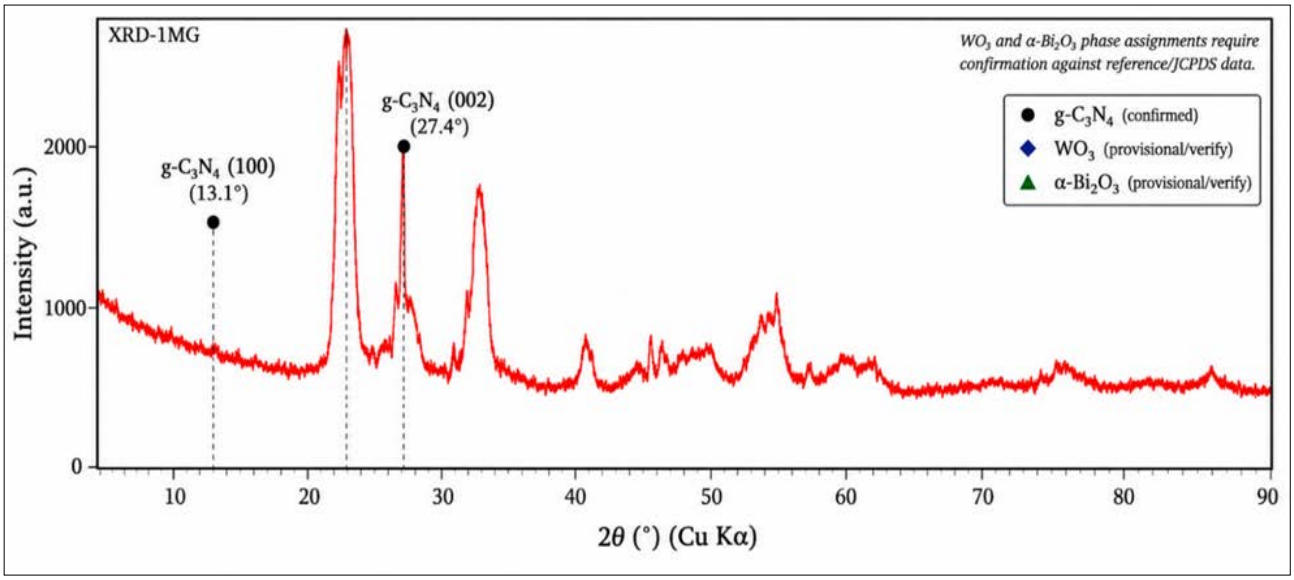


Fig 1: XRD of ternary composite

1.2 FTIR Analysis

The functional groups and chemical bonding of the synthesized g-C_3N_4/WO_3/Bi_2O_3 composite were examined by Fourier transform infrared spectroscopy (FTIR), and the corresponding spectrum is shown in Figure 2.

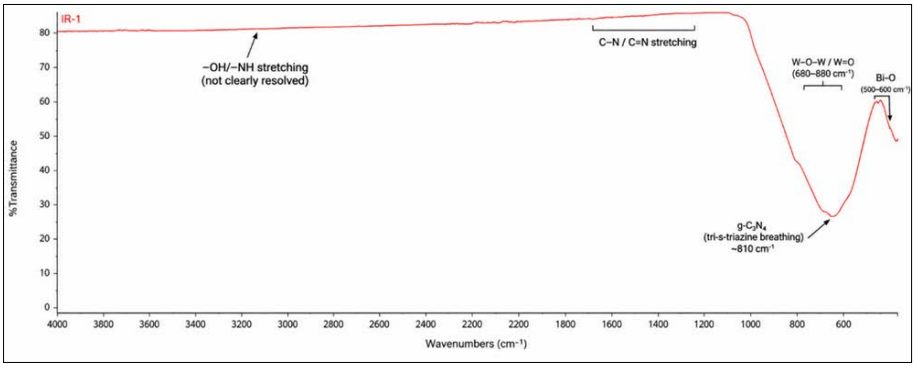


Fig 2: FTIR of ternary composite

1.3 FESEM Analysis

The surface morphology of the synthesized g-C_3N_4/WO_3/Bi_2O_3 composite was examined by FESEM, and the corresponding micrographs are presented in Figure 3.

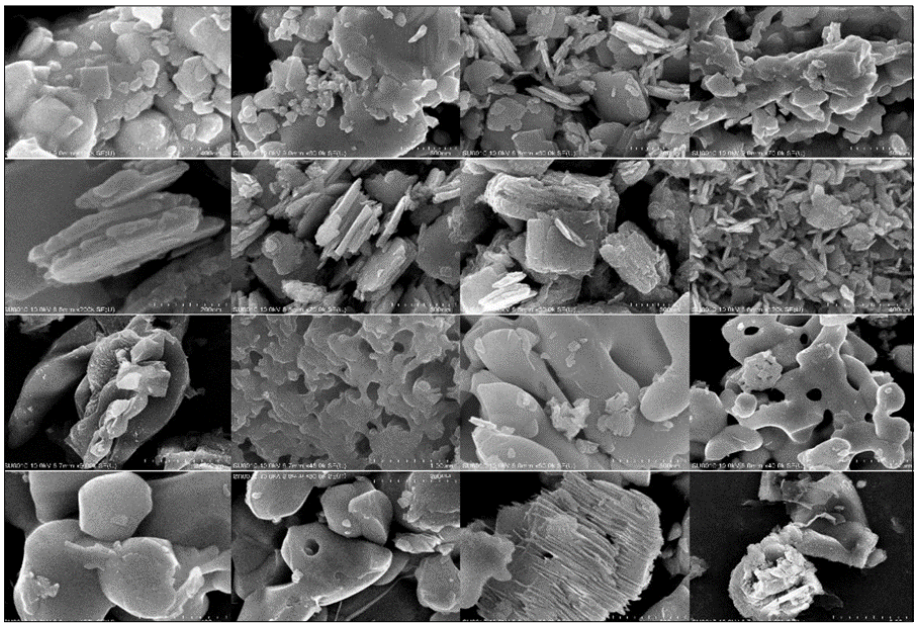


Fig 3: FESEM analysis of ternary composite

1.4 EDX analysis

The elemental composition of the synthesized g-C_3N_4/WO_3/Bi_2O_3 composite was examined by energy-dispersive X-ray spectroscopy (EDS), and the corresponding spectrum is presented in Figure 4.

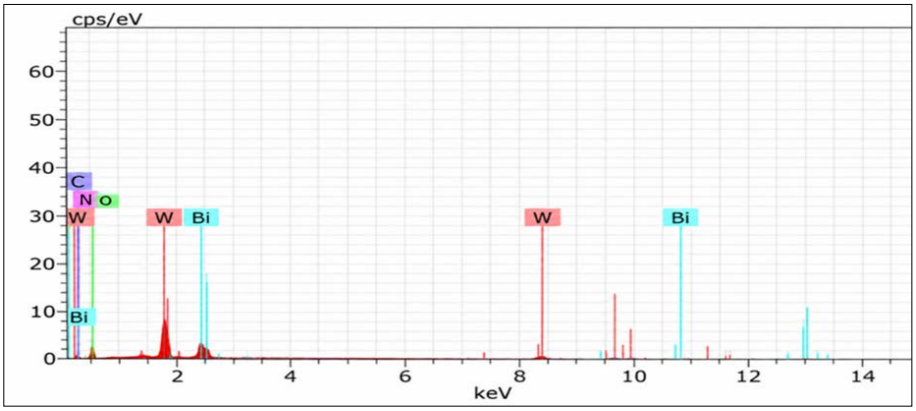


Fig 4: EDX analysis of ternary composite

1.5 UV–Vis Diffuse Reflectance Spectroscopy (DRS) Analysis

The optical properties of the synthesized g-C_3N_4/WO_3/Bi_2O_3 composite were investigated by UV–Vis diffuse reflectance spectroscopy (DRS), and the corresponding spectrum is presented in Figure 5.

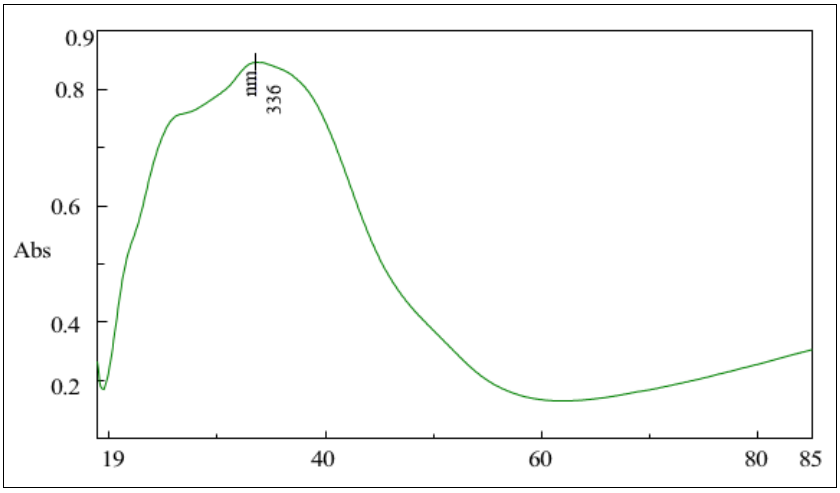


Fig 5: UV-VIS analysis of ternary composite

1.6 Band gap Study via Tauc Plot

Absorption spectra have been recorded out using a UV-vis spectrophotometer. It represents the Tauc plot equation is$((\alpha h\nu)^2$ vs hν). It exposed that the band gap of g-C_3N_4/WO_3/Bi_2O_3 composite was spotted at 2.62 eV. The photon energy is calculated and is hν (eV) = 1239.84 / λ (nm). It can be employed in visible light photocatalytic reactions. (Figure 6)

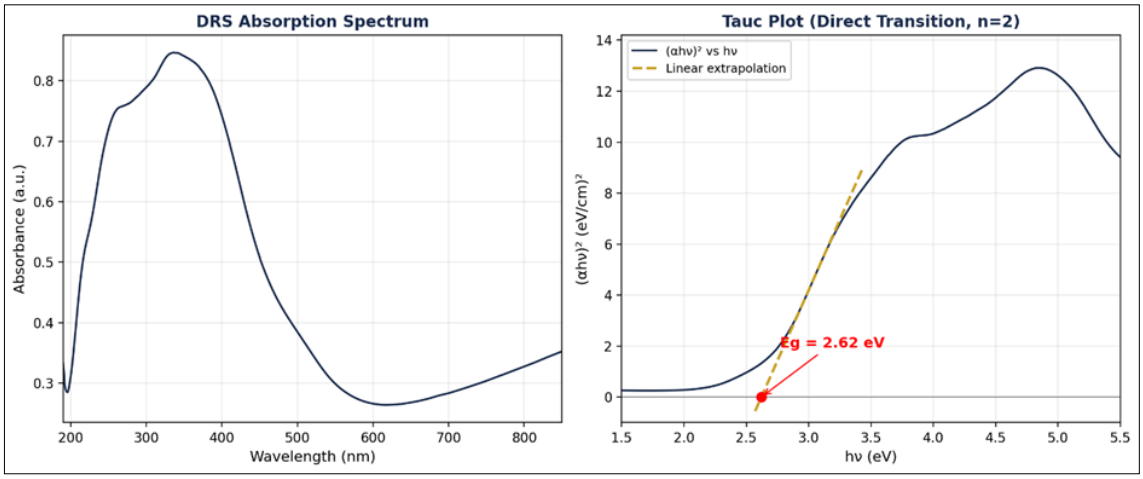
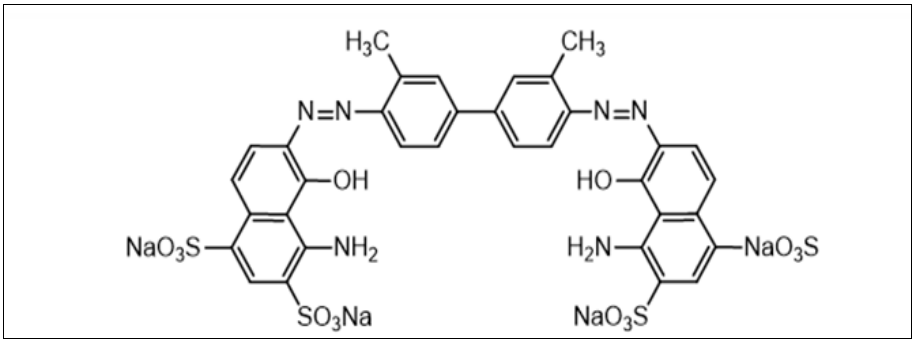


Fig 6: Tauc plot of ternary composite

2. Evaluation of photocatalytic act of ternary g-C_3N_4/WO_3/Bi_2O_3 nanocomposite

2.1 Degradation of Evans Blue under Optimized Conditions

Evans Blue, T-1824 or Direct Blue 53 an azo dye (Figure 7), was used as the pollutant to study the visible-light photocatalytic activity of the fabricated g-C_3N_4/WO_3/Bi_2O_3 composite due to its high stability and widely used in biomedical and physiological research. The photocatalytic degradation experiments were performed under the optimized conditions of pH 7.5, initial dye concentration of 0.4 mg L^{-1}, catalyst dosage of 0.06 g per 100 mL, and light intensity of 60 mW cm^{-2}



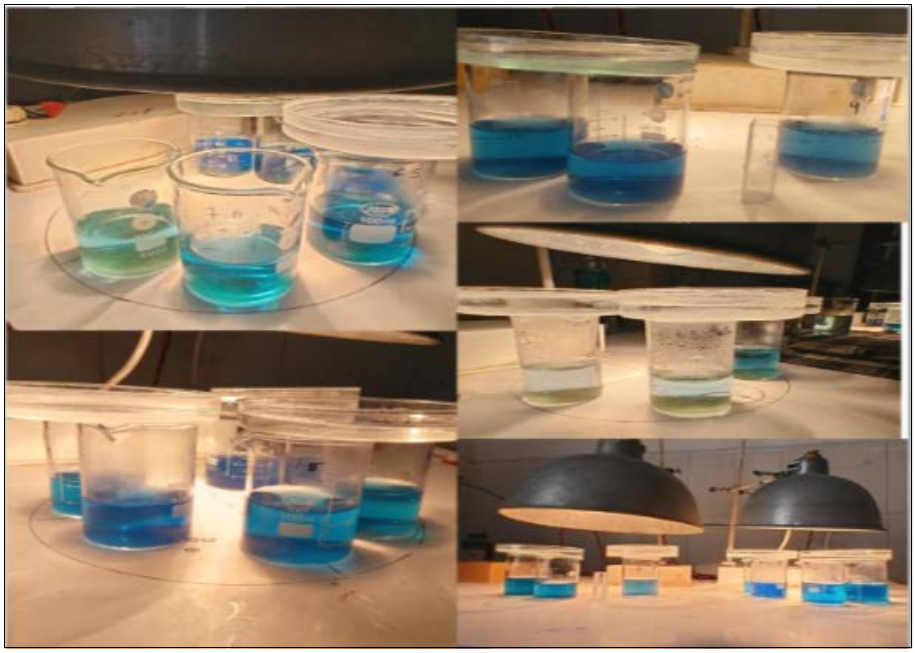


Fig 7: Structure and experiment view of Evans Blue dye

As irradiation time increased, the absorbance of Evans Blue gradually decreased from 0.986 to 0.101 over 190 min, corresponding to a degradation efficiency of approximately 89.75%. The continuous decline in absorbance indicates the progressive decomposition of Evans blue molecules under visible-light irradiation in the presence of the g-$C_3N_4/WO_3/Bi_2O_3$ photocatalyst.

The degradation kinetics followed a pseudo-first-order model, depicted by the linear relationship between (1 + log A) and irradiation time (Figure 8) (Table 2). The data points of the typical photocatalytic runs presented in Figure 7 are provided in the supplementary file as Table 2.

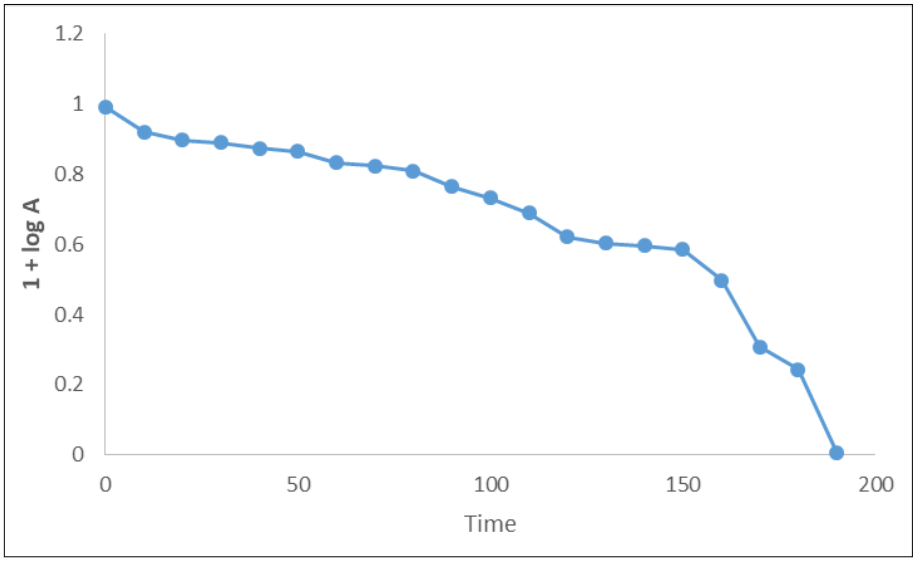


Fig 8: 1+log A vs. time plots for photocatalytic degradation of Evans blue under optimal conditions.

Table 2: A Typical Run of Evans Blue

Time	Absorbance	1 + log A
0	0.986	0.993
10	0.832	0.92
20	0.792	0.898
30	0.778	0.89
40	0.75	0.875
50	0.736	0.866
60	0.682	0.833
70	0.667	0.824
80	0.645	0.809
90	0.583	0.765

100	0.54	0.732
110	0.489	0.689
120	0.419	0.622
130	0.401	0.603
140	0.396	0.597
150	0.385	0.585
160	0.315	0.498
170	0.203	0.307
180	0.175	0.243
190	0.101	0.004

2.2 Kinetic Parameters Summary

The optimized reaction parameters and kinetic data for the photocatalytic degradation of Evans Blue dye using the g-$C_3N_4/WO_3/Bi_2O_3$ nanocomposite are summarized in Table 3. The photocatalytic performance was evaluated by varying key experimental parameters, including pH, initial dye concentration, catalyst dosage, and light intensity. Under optimized conditions, the composite exhibited efficient degradation of Evans Blue with a corresponding rate constant of $24.82 \times 10^{5}\ s^{-1}$.

Table 3: Optimized parameters and kinetic data for photocatalytic degradation of Evans Blue

Parameter	Evans Blue	**Unit**
Optimal pH	8.0	—
Dye Concentration	0.4	mg/L
Catalyst Dose	0.06	g/100 mL
Light Intensity	60	$mWcm^{-2}$
k (rate constant)	$24.82\times 10^{5}\ s^{-1}$	s^{-1}
Degradation	~90%	%

2.3 Effect of pH

Solution pH profoundly influences photocatalytic performance by altering the surface charge of the catalyst, the ionization state of the dye, and the availability of hydroxyl radicals. Figure 8 presents the pseudo-first-order rate constants as a function of pH for this dye. Table 4 contains the pH variation data and corresponding rate constant values used for the kinetic analysis presented in Figure 9 (a). For Evans Blue, the rate constant increased from $14.07 \times 10^{5}\ s^{-1}$ at pH 5.0 to a maximum of $24.82 \times 10^{5}\ s^{-1}$ at pH 8.0, declining at higher pH values. [+]

Table 4: Effect of pH on pseudo-first-order rate constant k for Evans Blue degradation

pH	**$k \times 10^{5}\ s^{-1}$**
5	14.07
5.5	14.39
6	14.71
6.5	16.79
7	17.98
7.5	19.90
8	24.82
8.5	21.91
9	20.11
9.5	16.19
10	14.93

3.4 Effect of Initial Dye Concentration

The initial dye concentration governs the number of reactive species available relative to the photocatalyst surface area and incident photons. Figure 9 (b) shows the dependence of K on dye concentration. For Evans Blue, the highest rate constant ($24.82 \times 10^{5}\ s^{-1}$) was obtained at 0.4 mg/L corresponds to Table 5. At low concentrations, an insufficient number of dye molecules adsorb onto the catalyst surface, while at high concentrations (>0.2 Mg/L), the excess dye molecules compete for active sites and may act as inner filters by absorbing incident photons, reducing catalyst activation. This behavior aligns with Langmuir–Hinshelwood kinetics.

Table 5: Effect of initial dye concentration on pseudo-first-order rate constant k for Evans Blue degradation.

Concentration of dye (mg/L)	**$k \times 10^{5}\ s^{-1}$**
0.2	13.96
0.4	24.82
0.6	21.87
0.8	19.70
1	15.80
1.2	13.41
1.4	11.94

3.5 Effect of Catalyst Dosage

Catalyst dose gives the number of active surface sites. As shown in Figure 5, for Evans Blue, k increased from $15.58 \times 10^{5}\ s^{-1}$ at 0.02 g to a maximum of $24.82 \times 10^{5}\ s^{-1}$ at 0.06 g, then declined at higher loadings. This well-documented phenomenon in photocatalytic systems results in decreased degradation efficiency at higher catalyst concentrations Figure 9(c). The corresponding experimental data are provided in the supplementary information Table 6.

Table 6: Effect of catalyst dosage on photocatalytic rate constant (k) for Evans Blue

Catalyst (g)	**$k \times 10^{5}\ s^{-1}$**
0.02	15.58
0.04	18.02
0.06	24.82
0.08	20.67
0.1	19.35
0.12	14.53

3.6 Effect of Light Intensity

Light intensity directly controls the rate of electron-hole pair generation. As shown in Figure 6, dye exhibits enhance degradation rates with increasing light intensity, consistent with increased photon flux and consequently greater generation of reactive oxygen species (ROS). For Evans Blue, k increased progressively from $13.83 \times 10^{5}\ s^{-1}$ at 20 $mWcm^{-2}$ to $24.82 \times 10^{5}\ s^{-1}$ at 60 $mWcm^{-2}$ and declining to $18.63\times 10^{5}\ s^{-1}$ at 70 $mWcm^{-2}$.

For Evans Blue, the maximum rate constant (k) was observed at an optimum light intensity of 60 mW cm^{-2} ($24.82 \times 10^{5}\ s^{-1}$). The corresponding kinetic data for different light intensities are provided in the supplementary information Table 7, and the graphical representation is shown in Figure 9(d).

Table 7: Effect of light intensity on photocatalytic rate constant (k) for Evans Blue

Light intensity (mWcm $^{-2}$)	**k ×10^{5}** s ^{1}
20	13.83
30	17.67
40	19.51
50	20.23
60	24.82
70	18.63

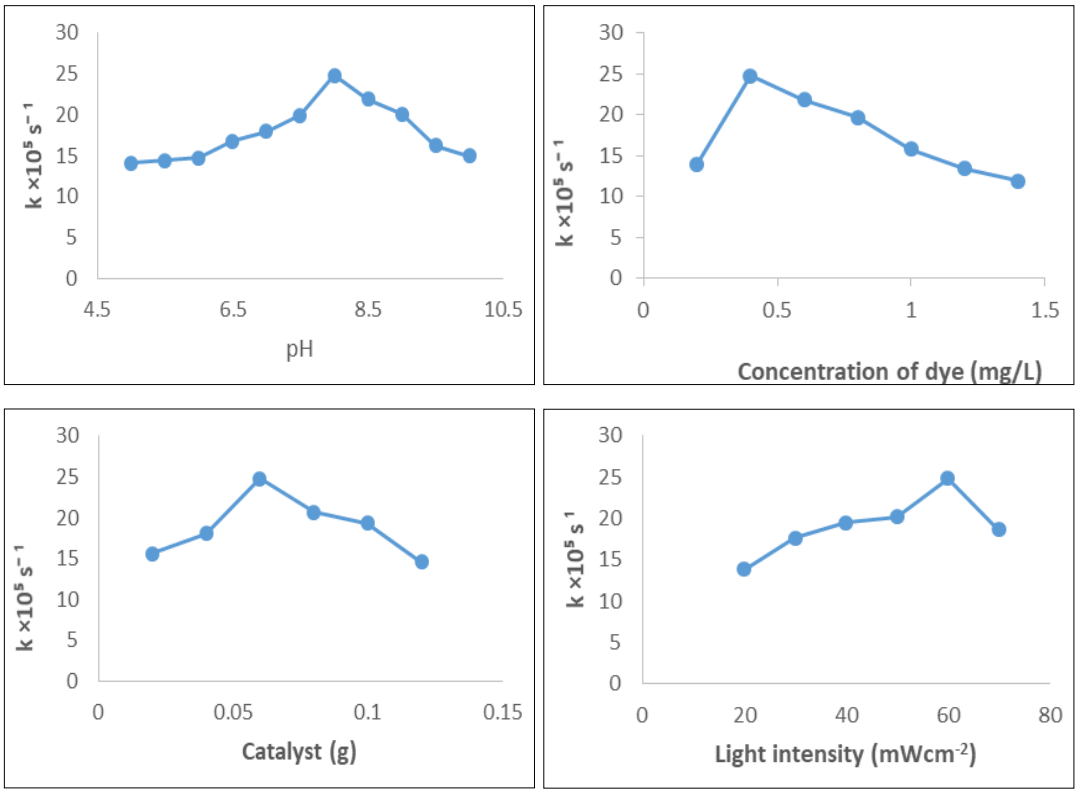


Fig 9: Effect of various parameters: (a) Effect of solution pH, ((b) Effect of initial dye concentration, (c) Effect of catalyst dosage, (d) Effect of light intensity on pseudo-first-order rate constant (k) for Evans Blue

Proposed Photocatalytic Mechanism

Based on the experimental evidence, a dual Z-scheme charge transfer mechanism is proposed for the g-C_3N_4 /WO_3 /Bi_2O_3 ternary composite, as illustrated schematically in Figure 11. Upon visible light irradiation, all three semiconductors are simultaneously photoexcited, generating electron (e^-) and hole (h^+) pairs.

The conduction band (CB) and valence band (VB) of the components are: g-C_3 N_4 (CB: −1.1 eV, VB: +1.6 eV), WO_3 (CB: +0.5 eV, VB: +3.2 eV), and Bi_2 O_3 (CB: +0.33 eV, VB: +3.13 eV). In the dual Z-scheme configuration: (i) electrons from the CB of WO_3 recombine with holes in the VB of g-C_3 N_4 at the g-C_3 N_4 /WO_3 interface; (ii) electrons from the CB of Bi_2 O_3 recombine with holes in the VB of WO_3 at the WO_3 /Bi_2 O_3 interface. This transfer preserves the electrons in the CB of g-C_3 N_4 (high reductive potential) and holes in the VB of Bi_2 O_3 (high oxidative potential).

The accumulated electrons in the CB of g-C_3 N_4 reduce dissolved O_2 to superoxide radicals (■O_2^-), which may further react to produce H_2 O_2 and ■OH. Simultaneously, the holes in the VB of Bi_2O_3 oxidize adsorbed water or surface hydroxyl groups to generate ■OH radicals.

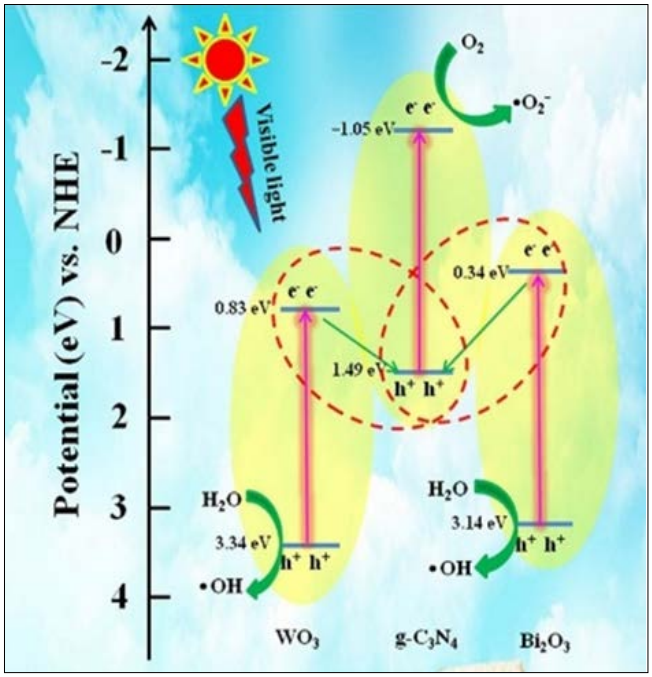


Fig 11: Proposed dual Z-scheme photocatalytic mechanism for g-C_3N_4/WO_3/Bi_2O_3 composite showing charge transfer pathways and reactive oxygen species generation.

$g\text{-}C_3N_4/WO_3/Bi_2O_3 + h\nu \rightarrow e^-(g\text{-}C_3N_4) + h^+(Bi_2O_3)$

$e^-(g\text{-}C_3N_4) + O_2 \rightarrow \blacksquare O_2^- \rightarrow \blacksquare OH + H_2O_2$

$h^+(Bi_2O_3) + H_2O / OH^- \rightarrow \blacksquare OH$

$\blacksquare OH / \blacksquare O_2^- / h^+ + Dye \rightarrow CO_2 + H_2O + Mineral\ ions$

Conclusion

A ternary $g\text{-}C_3N_4/WO_3/Bi_2O_3$ photocatalyst via a dual Z-scheme charge-transfer mechanism was constructed and estudied for the visible-light-driven degradation of the diazo dye Evans Blue. The optimized conditions (pH 8.0, dye concentration of 0.4 mg L^{-1}, catalyst dosage of 0.06 g, and light intensity of 60 mW cm^{-2}) confirms it as an excellent photocatalytic performance. The effective activity of the ternary heterojunction improves efficient charge separation, visible-light absorption, and reduces electron–hole recombination via dual Z-scheme mechanism. Future work should also scale-up under natural solar irradiation, identification of degradation intermediates and their toxicity.

Acknowledgements

The authors gratefully acknowledge the PAHER University, Udaipur (Raj) India for providing laboratory facilities. The authors also thank the Sophisticated Analytical Instrumentation Facility, Panjab University, Chandigarh, India for XRD, FTIR, FESEM, and EDX analysis.

No conflict of interest is declared.

References

1. Basirun A, Othman AR, Yasid NA, Halmi MIE, Gunasekaran B, Abd Shukor MY. Adsorption kinetics, equilibrium, and thermodynamic studies to understand adsorption behavior of Evans blue dye by durian husk. Korean J. Chem. Eng.,2023:40(6):1440–1456. doi.org/10.1007/s11814-023-1434-y.
2. Fujishima A, Honda K. Electrochemical photolysis of water at a semiconductor electrode. Nature,1972:238(5358):37–38. doi.org/10.1038/238037a0.
3. Berekute K, Yu KP, Chuang YHB. Enhanced photocatalytic activity of novel α Bi_2O_3@g-C_3N_4 composites for the degradation of endocrine-disrupting benzophenone-3 in water under visible light. Sustain. Environ. Res.,2022:32(1):17. doi.org/10.1186/s42834-022- 00127-2.
4. Fernandes E, Gomes J, Martins RC. Semiconductors application forms and doping benefits to wastewater treatment: A comparison of TiO_2, WO_3, and g-C_3 N_4. Catalysts, 2022, 12(10). doi.org/10.3390/catal12101218
5. Yang H, Lin J, Wen Z, Li Z, Zeng J, Wang L, *et al*. ZnS/CuFe2O4/MXene ternary heterostructure photocatalyst for efficient adsorption and photocatalytic degradation of azo dyes under visible light: Synergistic effect, mechanism, and application. Chemosphere,2023:339:139797. doi.org/10.1016/j.chemosphere.2023.139797.
6. Zhang J, Hu Y, Jiang X, Chen S, Meng S, Fu X. Design of a direct Z-scheme photocatalyst: Preparation and characterization of Bi2O3/g-C3N4 with high visible light activity. J. Hazard. Mater.,2014:280:713–722. doi.org/10.1016/j.jhazmat.2014.08.055.
7. Jiang LB, Yuan XZ, Zeng GM, Liang J, Chen XH, Yu HB, *et al*. In-situ synthesis of direct solid-state dual Z-scheme WO3/g-C3N4/Bi2O3 photocatalyst for the degradation of refractory pollutant. Appl. Catal. B: Environ.,2018:227:376–385. doi.org/10.1016/j.apcatb.2018.01.042.
8. Mostafa MR, Moustafa SA, Mohamed GG, Fouad OA. Kinetics and adsorption isotherms studies for the effective removal of Evans blue dye from an aqueous solution utilizing for sterite nanoparticles. Sci. Rep.,2024:14:24392. doi.org/10.1038/s41598-024-73697-x.
9. Sher M, Javed M, Shahid S, Iqbal S, Qamar MA, Bahadur A, *et al*. The controlled synthesis of g-C3N4/Cd doped ZnO nanocomposites as potential photocatalysts for the disinfection and degradation of organic pollutants under visible light irradiation. RSC Adv., 2021. doi.org/10.1039/D0RA08573A.
10. Abdollahpour R, Bazyari A. Synergistic photocatalysis: enhanced degradation of organic dyes using a heterojunction nanocomposite of high-surface-area g-C3N4 and TiO2− WO3− Bi2O3/SiO2. Env. Sci. Poll. Res.,2025:32(29):17466-17486.
11. Ameta R, Punjabi PB, Ameta SC. Photodegradation of naphthol green B in the presence of semiconducting antimony trisulfide. J. Serb. Chem. Soc.,2011:76(7):1049-1055.
12. Boddepalli R, Gurugubelli TR, Netheti VB, Alharthi SS, Koutavarapu R, Pidaparthy LS. A dual Z-scheme g-C¬3N4/SnWO4/CeO2 ternary heterostructure for enhanced visible light photocatalytic degradation of emerging pollutants. Surf. Interfaces, 2026, 110228. doi.org/10.1016/j.surfin.2026.110228.
13. Martínez-López S, Lucas-Abellán C, Serrano-Martínez A, Mercader-Ros MT, Cuartero N, Navarro P, *et al*. Pulsed light for a cleaner dyeing industry: Azo dye degradation by an advanced oxidation process driven by pulsed light. J. Clean. Prod.,2019:217:757-766. doi.org/10.1016/j.jclepro.2019.01.230.
14. Ong WJ, Tan LL, Ng YH, Yong ST, Chai SP. Graphitic carbon nitride (g-C_3N_4) based photocatalysts for artificial photosynthesis and environmental remediation: Are we a step closer to achieving sustainability? Chem. Rev.,2016:116(12):7159–7329.
15. Wang W, Liu X, Li Z, Luo H, Meng Z, Wang H, *et al*. Efficiency and mechanistic insights of photocatalytic degradation and sterilization utilizing g-C3N4/WO3-x Z-scheme heterojunction under full-spectrum light. J. Env. Chem. Eng., 2024, 12(6). doi.org/10.1016/j.jece.2024.114392.
16. Wang X, Maeda K, Thomas A, Takanabe K, Xin G, Carlsson JM, *et al*. A meta l-free polymeric photocatalyst for hydrogen production from water under visible light. Nat. Mater.,2009:8(1):76–80.
17. Zheng X, Han H, Zhang R, Yang J. Construction and photocatalytic performance of dual Z-scheme BiVO4/AgBr/Ag2MoO4 heterojunction for enhanced photocatalytic degradation of rhodamine B. J. Chem. Phys., 2026, 113112. doi.org/10.1016/j.chemphys.2026.113112.
18. Galavidoost Y, Habibi-Yangjeh A, Pournemati K, Khataee AA. Combination of oxygen-vacancy-rich TiO2− x with WS2/Co3S4/Co9S8 for photocatalytic degradation of effluents boosted by dual Z-scheme carriers transfer. J. Water Process Eng.,2026:85:109724. doi.org/10.1016/j.jwpe.2026.109724.

19. Li Y, Zhang H, Zhang D, Yao S, Dong S, Chen Q, *et al*. Construction of Bi2WO6/g-C3N4 Z-scheme heterojunction and its enhanced photocatalytic degradation of tetracyc202ne with persulfate under solar light. Molecules,2024:29(5):1169. doi.org/10.3390/molecules29051169.
20. Wang Z, Dou M, Li Y, Kong L, Yang H, Chen YY, *et al*. Construction of WO3/BiOBr/g-C3N4 double Z-scheme heterojunction for the photocatalytic degradation of tetracycline and reduction of U (VI). J. Alloys Comp., 2025, 1010. doi.org/10.1016/j.jallcom.2024.177420.